

Hydrothermal deactivation of silica-supported cobalt catalysts in Fischer–Tropsch synthesis

Gabor Kiss,^{a,*} Chris E. Kliewer,^a Gregory J. DeMartin,^a Claude C. Culross,^b and Joseph E. Baumgartner^a

^a *ExxonMobil Research and Engineering Company, Corporate Strategic Research, 1545 Route 22 East, Annandale, NJ 08801, USA*

^b *ExxonMobil Refining and Supply Co., Process Research Laboratories, PO Box 2226, Baton Rouge, LA 70821, USA*

Received 17 September 2002; revised 16 January 2003; accepted 4 February 2003

Abstract

Hydrothermal conditions created by high conversion in Fischer–Tropsch hydrocarbon synthesis induce cobalt–silica mixed oxide formation causing deactivation of silica-supported cobalt catalysts. The mixed oxide phase displays a distinctive needle-like morphology with a 1-nm lattice spacing and has a Co/Si atomic ratio of 1.2/1. The hydrothermal origin of the mixed oxide is confirmed by the fact that steamed catalyst samples contain the same needle-like phase with identical lattice spacing and Co/Si ratio. Reduction in 1.2 MPa H₂ at ≥ 400 °C decomposes the mixed oxide and recovers small metallic cobalt particles.

© 2003 Elsevier Science (USA). All rights reserved.

Keywords: Fischer–Tropsch synthesis; Silica-supported cobalt catalyst; Cobalt–silica mixed oxide formation; Hydrothermal deactivation; Reductive regeneration

1. Introduction

Cobalt-catalyzed Fischer–Tropsch (FT) synthesis converts natural gas to hydrocarbon liquids with high carbon efficiency due to the low water–gas shift activity of the catalyst. Using decane as a representative hydrocarbon product of the hydrocarbon synthesis process, methane conversion to liquid hydrocarbons via autothermal reforming and FT synthesis can be written as follows:



While cobalt-catalyzed FT synthesis is advantageous in carbon utilization as compared to processes using iron, cobalt is more expensive necessitating longer catalyst life [1]. Catalyst stability therefore is an important performance variable in cobalt-catalyzed FT processes.

Cobalt catalysts seem to undergo various intrinsic deactivation processes during FT synthesis. Thus, for example, refractory carbon buildup on the active metal surface was pro-

posed as a deactivation channel in CO hydrogenation. Deactivation by some sort of refractory carbonaceous phase has been widely postulated [2–9]. This mechanism, however, is hard to unequivocally prove in FT synthesis due to the presence of heavy hydrocarbon wax product and the potential buildup of inert carbon on the catalyst support.

Of the different forms of carbonaceous species potentially capable of reducing catalyst activity in FT, two seem to be harmless:

- A surface science study of CO and CO₂ hydrogenation by cobalt shows that carbon deeply penetrates into the bulk metal [10]. This dissolved carbon is readily hydrogenated forming methane and C₂+ hydrocarbon.
- DOE researchers tested the hypothesis that pore plugging by the heavy wax product leads to deactivation. They found that toluene extraction did not restore catalyst activity and thus rejected the possibility of deactivation by pore blockage [2].

Despite these recent results, the formation of other, more refractory surface-blocking carbon cannot be excluded.

Water is known to affect the kinetics and selectivity of cobalt-catalyzed FT synthesis [11–22]. More recently,

* Corresponding author.

E-mail address: gabor.kiss@exxonmobil.com (G. Kiss).

water also emerged as an important intrinsic factor inducing multiple deactivation processes. One of these deactivation mechanisms is believed to involve surface oxidation of the highly dispersed cobalt particles [11,12,23–31].

Hydrothermal conditions created by high CO conversion in hydrocarbon synthesis at elevated total pressures apparently facilitate reactions between some oxide supports and cobalt. Alumina-supported cobalt catalysts, for example, form difficult to reduce cobalt–alumina mixed oxide at CO conversion levels that generate several bars of steam pressure [12,23,24,26,32]. Recent studies [25,33] indicate that ZrO₂ coating reduces the interaction between cobalt and alumina, affording higher stable activity at commercially relevant pressures and conversions. It is also well known that unmodified SiO₂ supports are hydrothermally unstable [34–44]. A number of publications [34–41] describe cobalt silicate formation and support restructuring during catalyst preparation. ZrO₂, TiO₂, and ThO₂ modification of SiO₂ supports affords increased cobalt reducibility and higher FT activity [40,41] possibly by preventing mixed oxide formation. More recently, deactivation in hydrocarbon synthesis due to cobalt silicate formation and support sintering was also invoked [42–44]. It seems that both mixed oxide formation and support sintering are more pronounced with highly dispersed phases of cobalt and/or silica [38,42].

Earlier studies on the hydrothermal deactivation of silica-supported cobalt catalysts in FT synthesis used temperature-programmed reduction (TPR) to detect the formation of a more difficult to reduce phase [43,44]. These post-run TPR results are compelling but cannot tell how much of the deactivation observed in the catalytic run is caused by the formation of the cobalt phase reduced at higher temperatures nor can they reveal the chemical nature of these phases. By the combination of catalytic tests and electron microscopy methods, we now offer direct evidence for the formation of a cobalt–silica mixed oxide phase. We also discuss the effect of synthesis conditions and show that the deactivation-causing mixed oxide can be re-reduced in H₂ to cobalt metal and silica allowing the regeneration of the catalyst.

2. Experimental

2.1. Catalyst preparation

A solution of 5741 g of Co(NO₃)₂ · 6H₂O (Aldrich), 1224 g of ethylene glycol (Aldrich), and 208 g of perrhenic acid¹ (72.1%, Sandvik Rhenium Alloys) was prepared by heating the wet solid to 40 °C. This solution was blended to a thin paste with 1000 g of EH-5 fumed silica (Cabot) in a Hobart mixer. The paste was calcined in air at 400 °C for 1 h. The calcined catalyst was milled for 1 h to convert the soft cakes of catalyst to powder. The yield of the 400 °C-

calcined sample was 2629 g. Fifteen grams of the 400 °C-calcined catalyst was vacuum-annealed at 700 °C for 1.5 h. After cooling, 13.65 g of catalyst was collected.

2.2. Catalyst testing

Catalyst tests were performed in a down-flow fixed bed or in a continuous-flow slurry autoclave reactor. The 0.5-inch o.d./0.43-inch i.d. stainless-steel reactor body of the fixed bed reactor had a 0.125-inch o.d. thermocouple well in the center. The thermocouple well housed eight thermocouples 1.5-inches apart. The eight thermocouples of the reactor were calibrated and certified by the vendor. The volume of the catalyst plus diluent bed positioned between the top and bottom thermocouples was 23 mL. The reactor vessel was sleeved in a 2.5-inch-diameter aluminum or brass cylindrical block to provide better heat distribution. Feed gas was fed to the catalyst bed through a 0.125-inch preheat tube housed in the brass or aluminum block to the feed introduction point at the top of the reactor. The reactor was heated by an infrared furnace and by a resistive auxiliary heater installed at the bottom of the brass (or aluminum) block. The latter was installed to ensure isothermal bed conditions. The catalyst bed was held in place by stainless-steel filter discs both on the bottom and the top.

The temperature of the reactor was controlled from the first and last thermocouples of the reactor bed. The bed temperatures at those two points therefore were always fixed at a given set value. The temperature of the internal bed zone (i.e., between the first and last thermocouples) was within 1 K of the set value in blank runs, i.e., without heat release from a reaction. In order to reduce the temperature spread in the catalyst bed during kinetic experiments, the catalyst was diluted with similarly sized quartz sand at a quartz-to-catalyst volume ratio of approx 8:1. The axial temperature spread in the catalyst bed under the Fischer–Tropsch condition was typically 3 to 10 K. The average temperature of the catalyst bed was calculated as a weighted average. The weighting factor for the first and last thermocouple zones (entrance and exit points) was set to one-half of that of the internal thermocouple zones.

Feed components were individually fed through Brooks mass-flow controllers. Chemically pure (CP grade) CO and Ar were purchased from MG Industries or BOC Gases. H₂ (99.995% purity, O₂ < 1 ppm) was fed from a central house supply. All three gases were purified with MG Industries' Oxisorb HP filters providing O₂ and H₂O levels below 0.1 and 0.5 ppm, respectively. The CO was passed through a 180 °C trap filled with Cu granules from Aldrich (Cat. No. 31,140-5) for Fe(CO)₅ removal. The mixed synthesis gas feed containing CO, H₂, and Ar (internal standard) in the ratio of approximately 65:31:4, respectively, was further purified with a ZnO–Al₂O₃–CaO bed (Strem Chemicals, Cat. No. 30-2700) kept at 200 °C for H₂S removal. A dual-stage ISCO pump provided optional cofeeding of water (N₂-purged, HPLC grade).

¹ Rhenium was used as a reduction promoter and dispersion aid [26,49].

Mass balances were taken every 2 h. They were based on feed flow rates from Brooks mass-flow controllers and feed and effluent gas analyses by a custom-modified (Wasson-ECE Instrumentation, Inc., Fort Collins, CO) HP 5890 gas chromatograph (GC). All flows were referenced against an argon internal standard. The mass-flow controllers were calibrated in house. The GC's were calibrated periodically using certified calibration master blends (Air Products). Releasing the reactor pressure to ambient through an oil-filled bubbler provided constant-volume gas sampling for the GC. The results were not corrected for the changes in the atmospheric pressure. The constant-pressure sampling allowed independent GC calibration and analysis for each component. Feed mass balances by the GC were typically $100 \pm 5\%$. Deviations between the feed concentrations calculated from the mass-flow controller values and the ones measured by GC were typically less than 10%. The GC calibration was checked and corrected whenever the deviation for the individual components and/or the feed balance fell outside the above ranges.

The unit was controlled by a Siemens/Texas Instruments programmable logic control computer (PLC). Process data were acquired automatically by a desktop personal computer (PC) via the PLC. The same PC also served as a PLC supervisor by downloading experimental protocols defined as pressure and temperature set values, ramp rates, and hold times. Another function of the supervisor PC was data acquisition from the GC using CHROM PERFECT software (Justice Innovations, Mountain View, CA). The process and GC data were automatically merged into EXCEL workbooks by an EXCEL macro.

In a typical fixed-bed experiment, 1.5–3 g of catalyst was diluted with quartz to 23-mL volume and charged into the reactor. The catalyst then was reduced in a flow of H_2 (450–475 standard mL/min) at 1.2 MPa by raising the temperature to 400–420 °C at a rate of 1 °C/min and holding the final temperature for 8 h. The catalyst was then cooled to 140–160 °C in flowing H_2 , put under 2 MPa of syngas ($H_2/CO \approx 2.1$) pressure, and, finally, brought up to synthesis temperature (200–220 °C) at a 1 °C/min ramp rate.

At the end of each kinetic run, the wax was removed by hydrogenolysis in flowing H_2 (400 standard mL/min) at 400 °C and 1.2 MPa H_2 pressure. The reactor body was disconnected and sealed under argon and the free-flowing catalyst bed was discharged inside a nitrogen-purged glove box. Catalyst samples were separated from the diluent using a rare-earth magnet in the glove box and were inertly transferred for subsequent characterization by TEM. Inert treatment of the spent catalyst samples prevented uncontrolled oxidation during discharge and allowed meaningful post-run catalyst characterization.

The 1 L Parr autoclave was heated in a circulated hot-air oven. The temperature of both the slurry and the gas phase was monitored by thermocouples mounted through the reactor head. The catalyst was reduced in a fixed bed

reactor and then transferred after reduction under inert blanket into the autoclave. The vapor reaction products were removed overhead with the unreacted feed, while the liquid products were removed via a 2- μ m internal stainless-steel filter (Alltech, No. 9402). The typical catalyst charge was 5–10 g. The start-up liquid was 450–500 mL molten Fischer-Tropsch wax generated in previous runs. Unit control, experimental conditions, and mass balance protocols were identical to the ones described above for the fixed-bed experiments. All sample preparations and transfers were carried out under N_2 or Ar using standard inert handling techniques. Spent catalysts were solvent-extracted inside a nitrogen-filled glove box using anhydrous toluene or heptane packed under nitrogen (Aldrich).

Catalytic activity was calculated by using a proprietary kinetic model. The kinetic model allowed us to compare catalytic activities under different conditions. The reported catalytic activities are relative values referenced to the measured initial activity obtained in the same test. The kinetic data described in the paper were obtained in three runs: fixed-bed runs 1 and 2 (FBR1 and FBR2) and an autoclave run. In order to aid discussion, different segments of the fixed bed runs are designated by a segment number reflecting chronological order. Thus, for example, FBR1_S1 represent data obtained in the first segment of fixed-bed run 1.

2.3. Transmission electron microscopy (TEM) and particle size measurements

Free-flowing reduced catalyst powders were prepared in a nitrogen-filled glove box for characterization in the TEM by placing ~ 0.01 g of powder into an agate mortar and pestle. The powder was crushed into fine bits (< 100 nm thick). The fines were dusted onto a standard, 200 mesh, holey-carbon-coated TEM grid. The grid was inertly transferred into either a Philips CM12 TEM or a Philips CM200 TEM/STEM by using a nitrogen-purged glove bag attached to the TEM. Samples were examined in the bright-field imaging mode at an accelerating voltage of either 120 or 200 kV, respectively.

Images were collected from random areas within the reduced samples at “on screen” magnifications of $53,000\times$ in the Philips CM12 and $54,000\times$ in the Philips CM200. In all cases, the data were collected as digital images via a Gatan CCD system using v.2.5 of Gatan's Digital Micrograph program. Digital images were collected from ~ 20 randomly selected areas for the fresh catalyst and ~ 80 randomly selected areas for the spent samples. The Co metal particles were visually identified in each image, and a line drawing tool (available within Digital Micrograph) was used to manually mark the diameter of each metal particle. The measured diameter for each particle was automatically collected within the Digital Micrograph program.

The TEM analysis of the spent catalyst from one of the fixed-bed runs (FBR2_S3) showed a new phase with needle morphology. To determine whether or not the formation of

this needle-like phase was reversible, the catalyst on the TEM grid was hydrogen-treated using a specially designed reactor assembly described elsewhere [45]. Thus, a portion of the spent, air-passivated catalyst was crushed into a fine powder using an agate mortar and pestle. The fines were dusted onto a 200-mesh, holey-carbon-coated Mo grid and transferred into a Philips CM12 TEM. Areas of the catalyst were imaged and mapped (i.e., certain specific features and their locations identified) for subsequent reexamination. The catalyst was removed from the TEM and placed into the microscopy reactor where it was reduced by heating in flowing H₂ (20 mL/min) at a rate of 4 °C/min from ambient temperature to 420 °C and holding at 420 °C for 12 h. The grid was subsequently transferred under inert conditions back into a Philips CM12 TEM. The areas that were previously imaged and mapped prior to the re-reduction were imaged again and a particle size analysis was conducted on the re-reduced sample.

2.4. Energy-dispersive spectrometry (EDS) of Co–Re/SiO₂ catalyst samples

The needle-like phase in the spent catalyst sample was investigated in the TEM using energy dispersive spectroscopy. The spent Co–Re/SiO₂ was prepared for analysis following the method described above for the TEM samples. However, in this case, the catalyst was air-passivated first by letting air diffuse into the storage vial through its loosened screw cap. The air-passivated sample was transferred into a Philips CM200F TEM/STEM where it was examined at an accelerating voltage of 200 kV. The electron beam was condensed to form a small probe. The probe was placed onto portions of the needle-like phase that appeared to be well separated from the cobalt particles and the support. Spectral data were collected using a Princeton Gamma Tech Energy Dispersive Spectrometry system using the IMIX software package.

A steamed Co–Re/SiO₂ sample was prepared by the following procedure: 1.2 mL of fresh catalyst was first reduced in flowing H₂ (74 standard mL/min) at 400 °C (heating rate from ambient temperature to 400 °C of 1 °C/min) and 1 bar for 8 h. The catalyst was cooled back to ambient temperature in flowing H₂ by turning off the furnace. At room temperature, the reactor was first purged with Ar (100 standard mL/min) for 30 min and then was pressurized with Ar to 20 bar. After reaching 20 bar pressure, the reactor was heated up to 220 °C at 1 °C/min under flowing Ar. After reaching 220 °C, 0.07 mL/min water was fed in 100 standard mL/min Ar via a vaporizer into the reactor for 16 h. After 16 h, the water co-feeding was stopped and the reactor was purged with Ar for 1 h. The steamed sample then was cooled in flowing Ar and discharged in a glove box. An aliquot of the steamed sample was air-passivated as described above for the spent catalyst sample. This air-passivated steamed Co–Re/SiO₂ was prepared for TEM/EDS analysis by crushing it into fine bits using an agate mortar and pestle. The fines were dusted onto a standard, 200-mesh copper grid. The grid

was transferred into a Philips CM200F TEM/STEM and the sample was analyzed using EDS in a manner similar to the spent reactor sample.

2.5. X-ray diffraction (XRD) studies and thermogravimetric analyses (TGA)

Magnetically separated spent catalyst samples were analyzed by XRD and TGA. The XRD analysis was performed using a Rigaku D-Max diffractometer using monochromatic Cu-K_α radiation. TGA data were collected on a Mettler TA850 thermal analyzer interfaced to an Allen–Bradley PLC for automated gas switching. The PLC permitted an automated inert purge between reductive and oxidative atmospheres during a single experiment. Background runs were carried out for each experiment on an empty crucible to allow correction for buoyancy and other system errors. The spent catalyst sample (~70 mg) was first dried in Ar at 120 °C for 2 h. It then was reduced in 100% H₂ while heating at a rate of 4 °C/min to 500 °C and held for 1 h. The sample was then cooled to 25 °C and passivated first in a 1% air/inert stream then in 100% air. After passivation, the sample was heated at a rate of 4 °C/min to 500 °C in 100% air (no hold) and then cooled to ambient temperature. Based on experiments with fresh catalyst samples, such 500 °C air treatments convert all metallic cobalt to Co₃O₄, which is also the original state of cobalt in the fresh catalyst. After back-oxidation, the sample was reduced for the second time, using the reduction conditions applied first. The TGA of a fresh catalyst sample was also carried out applying the above reduction–oxidation–reduction (ROR) sequence to provide a comparison with the spent catalyst. All TGA measurements were carried out at 1 atm total pressure.

3. Results and discussion

Amorphous SiO₂ is a frequently used support in cobalt Fischer–Tropsch catalyst formulations [41]. However, as mentioned earlier, silica-supported cobalt catalysts in hydrocarbon synthesis have some hydrothermal stability issues [42–44]. Indeed, we found that fumed silica-supported cobalt catalysts deactivated at high (≥90%) CO conversions forming a needle-like crystalline cobalt–silica mixed oxide phase. The section below on the catalytic tests describes how deactivation was induced by increasing CO conversion or by cofeeding water. It also details the activity changes due to hydrogen treatments applied after deactivating the catalyst at high CO conversion. The second part of the discussion summarizes the results on the ex situ TEM, EDS, and TGA studies that identified the mixed oxide phase, determined its composition, and proved its decomposition at the reductive regeneration conditions applied in the catalytic tests.

Table 1
Characterization results for the 400 °C-calcined and 700 °C vacuum-annealed catalyst samples

	400 °C calcined	700 °C vacuum annealed
Co ^a (wt%)	44.03	46.69
Re ^a (wt%)	3.94	4.41
Co ₃ O ₄ diameter by XRD (nm)	10.8	16.8
Surface area ^b (m ² /g)	144	69
Pore volume ^b (mL/g)	0.541	0.548
O ₂ titration ($\frac{\text{g}_{\text{atom O}}}{\text{g}_{\text{atom Co}}}$)	0.624	0.295

^a By Galbraith.

^b By nitrogen porosimetry (Omnisorb).

3.1. Catalytic tests with Co–Re/SiO₂

The 700 °C vacuum annealing sintered both the cobalt particles and the support of the Co–Re/SiO₂ sample substantially (see third and last entries in Table 1). The catalytic tests were performed with the vacuum-annealed catalyst typically at 220 °C and 2 MPa total pressure with stoichiometric syngas feeds (H₂:CO ≈ 2.1:1; 4–6% Ar internal standard) in a fixed bed reactor (cf. Experimental). As shown in Fig. 1, the catalyst demonstrated stable activity at moderate (50–55%) CO conversion levels. We observed that fresh and regenerated Co–Re/SiO₂ catalyst samples typically lost 15–20% of their initial activity in fixed bed runs during the first few days under synthesis conditions. Data from that “deedging” period are not included in Fig. 1. Similar initial activity loss is often observed in cobalt-catalyzed

Fischer–Tropsch synthesis [1,12,28,31]. This initial activity loss could be caused by several factors, most notably by oxidation of the least stable segment of the cobalt particle population or by surface oxidation [11,12,23–31]. It is worth mentioning that while Re does not affect Co site activity [27–29], the presence of Re likely increases the size of the oxidative activity loss due to the higher dispersion of Re-promoted cobalt catalysts [26–28]. As Holmen et al. pointed out [26], the direct involvement of Re cannot be excluded either.

In another experiment (FBR2_S1), the catalyst was exposed to high CO conversion (most of the time > 90%) conditions for a total of 2 weeks. Fig. 2 demonstrates that in this operation regime, catalytic activity rapidly declined and lined out at lower levels whenever conversion was increased by reducing space velocity. In this regard, the Co–Re/SiO₂ catalyst behaved similarly to the alumina-supported catalysts tested by Holmen’s group [12,28,31], although, as will be discussed later, the underlying reasons could be different.

After spending nearly 2 weeks under high CO conversion conditions, the relative activity declined from a value of 0.86 to 0.36, reflecting a ~50% activity loss during that period. Fixed bed reference tests at moderate conversion levels demonstrated significantly higher stability with only moderate activity loss (see, for example, Fig. 1). The rapid activity decline, therefore, can be correlated with the exposure to high CO conversion levels.

It has been suggested that the activity loss observed during high CO conversion or water cofeeding with alumina-

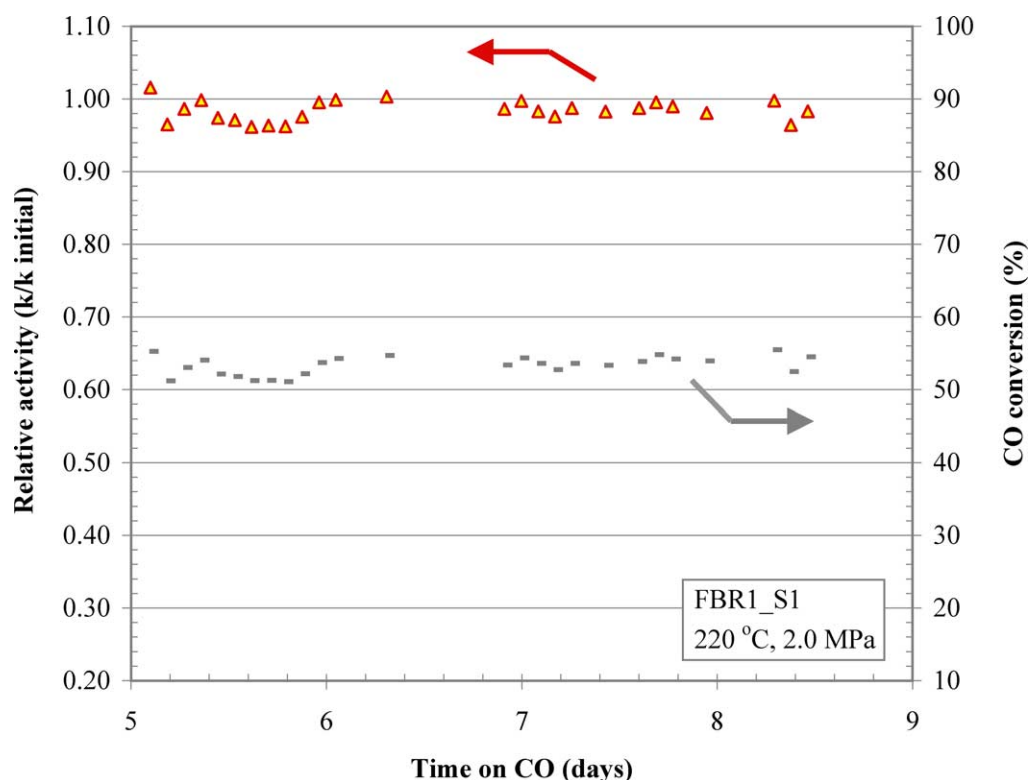


Fig. 1. The stability of the lined-out fresh Co–Re/SiO₂ catalyst at moderate conversion with stoichiometric feed (H₂:CO ≈ 2.1:1).

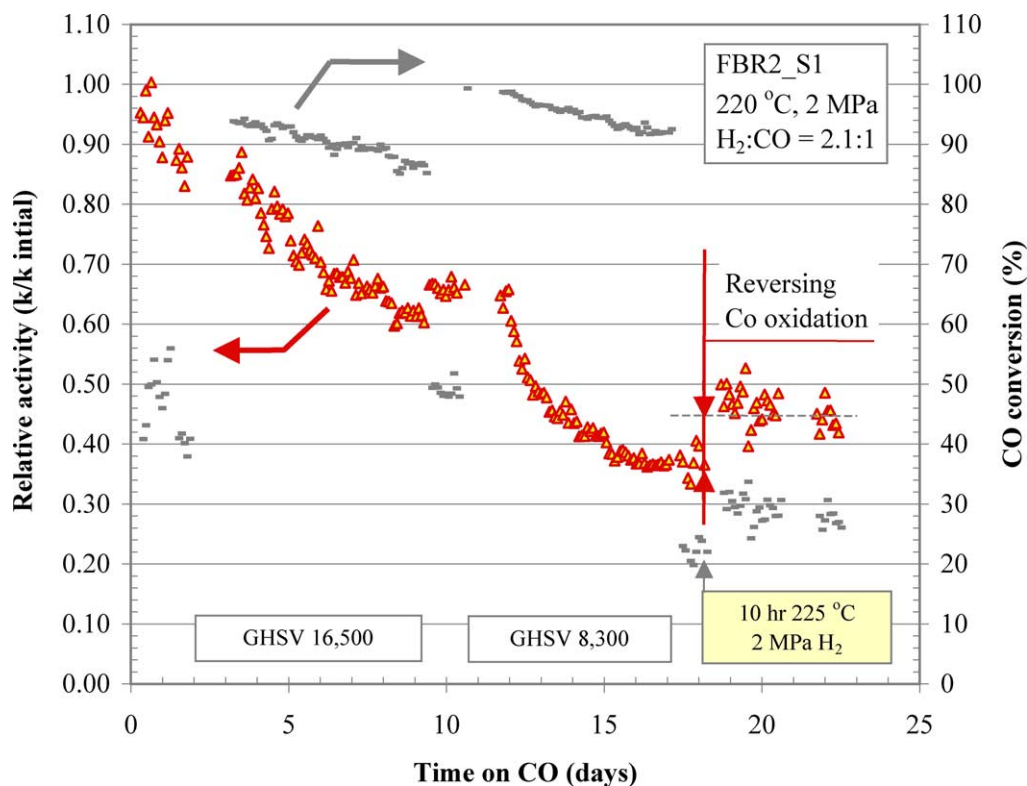


Fig. 2. Deactivation of Co-Re/SiO₂ at high CO conversion with stoichiometric feed ($H_2:CO \approx 2.1:1$) and the response of the deactivated catalyst to hydrogen treatment at Fischer-Tropsch synthesis temperature.

supported catalysts is due to active site loss caused by a combination of water-induced oxidation of cobalt and cobalt aluminate formation [12,23–31]. More recently, Bertole et al. [11] found that unlike in the case of alumina-supported cobalt catalysts, the primary reason for water-induced activity loss with unsupported Co is reduced site activity. The site activity loss reported in the later study was reversed by a 2-h hydrogen treatment at 250 °C and 2 MPa. Recent patent literature suggests that water-induced back-oxidation of cobalt supported on alumina [46] and ZrO₂-modified silica [47] can be largely reversed and catalytic activity can be recovered by hydrogen treatment at or close to the temperature and pressure of the hydrocarbon synthesis. Earlier publications generally imply that the deactivation process reversed by mild hydrogen treatment does not involve metal-support interaction but rather entails cobalt redox transformations with no support participation [11,12, 23–31]. We have carried out related studies, the results of which support this assessment.²

In order to estimate the fraction of the total activity loss caused by the above-discussed reversible cobalt redox process, a 10-h hydrogen treatment at 225 °C and 2 MPa was carried out at Day 18 in FBR2_S1. As shown in Fig. 2, this treatment recovered only a small fraction of the total activity loss, suggesting that in our study the bulk of the

deactivation caused by high CO conversion exposure was not due to the readily reversible cobalt oxidation. Indeed, as will be discussed later (vide infra), the rapid deactivation observed at high CO conversion was caused by the formation of a more refractory form of oxidized cobalt generated by cobalt-silica interaction.

The close correlation between increased steam pressure and deactivation was confirmed by water cofeeding experiments. For example, in one of our fixed bed experiments (FBR1_S2 shown in Fig. 3) we applied our standard synthesis conditions (220 °C, 2 MPa H₂/CO pressure) except that the total pressure was first raised from 2 to 2.5 MPa by cofeeding an additional 0.5 MPa Ar. As expected, the introduction of the extra Ar did not effect CO conversion and catalytic activity.³ After establishing the baseline CO conversion (moderate level, < 70%) and activity at 2.5 MPa total pressure, the 0.5 MPa Ar cofeed was intermittently replaced by ~0.5 MPa steam in the feed between Day 10 and Day 17 on CO. As depicted in Fig. 3, steam cofeeding at 50–70% CO conversion led to rapid catalyst deactivation that was also verified by returning to standard conditions at Day 17 using 2 MPa undiluted H₂/CO feed.⁴

³ FBR1_S2 shown in Fig. 3 is a continuation of FBR1_S1 in Fig. 1.

⁴ During steam cofeeding the CO conversion reversibly increased (see Fig. 3). For a detailed discussion of this well-known kinetic phenomenon in Co-catalyzed Fischer-Tropsch synthesis see [50,51].

² A manuscript on the later study will be submitted for publication shortly.

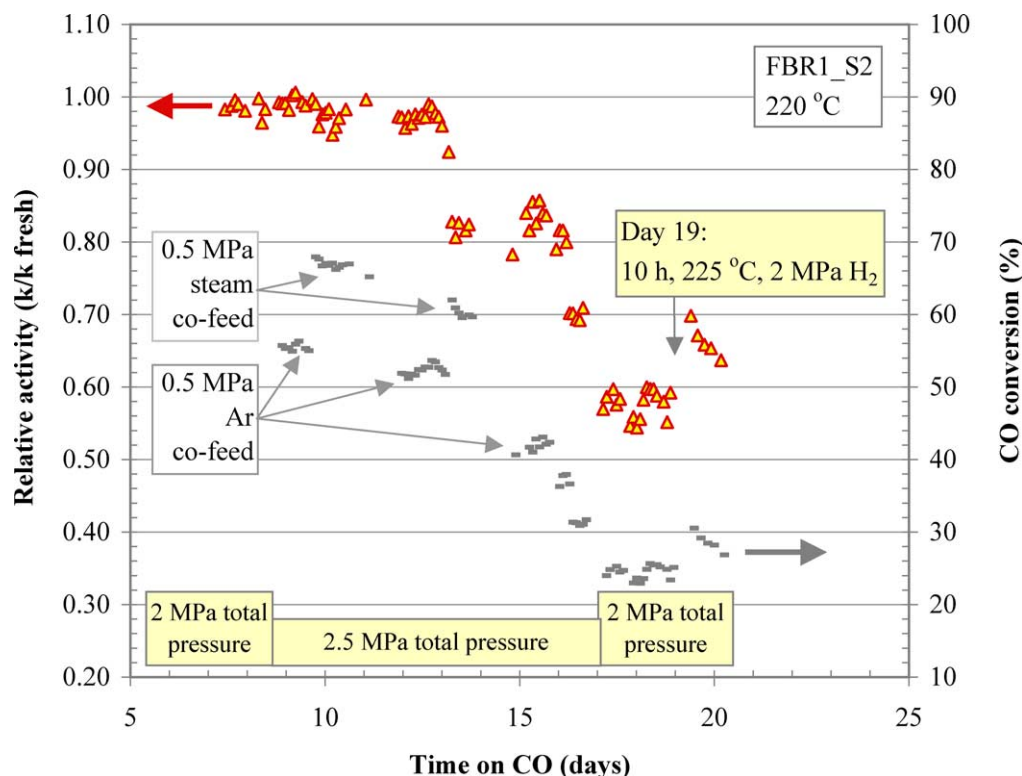


Fig. 3. Deactivation of Co–Re/SiO₂ during water cofeeding, and the response of the deactivated catalyst to hydrogen treatment at Fischer–Tropsch synthesis temperature.

After water cofeeding, the deactivated catalyst was hydrogen-treated under the same conditions (10 h, 2 MPa H₂ at 225 °C) as applied in the earlier-described high CO conversion test, FBR2_S1 (cf. Fig. 2). Just as after exposure to high CO conversion, this hydrogen treatment recovered only a small fraction of the total activity loss (see activity changes after the hydrogen treatment at Day 19 in Fig. 3). The similarities in the conditions causing deactivation and the responses to hydrogen treatment suggest that the deactivation processes observed at high CO conversion and during water cofeeding are the same. Further evidence for the common hydrothermal nature of the above-described deactivation process will also be provided later by comparing the morphology and composition of the phases formed at high CO conversion in FT synthesis and during catalyst steaming (vide infra).

Although hydrogen treatment at 225 °C did not regenerate catalytic activity after exposure to high CO conversion or water cofeeding, hydrogen treatment of similarly deactivated catalyst samples at 420 °C recovered all but a small fraction of the lost catalytic activity. Fig. 4 shows the results from one of these experiments, FBR2_S2. The baseline activity of the regenerated catalyst was first established at lower than 90% CO conversion levels during the first week of the experiment. After this first week on synthesis, the conversion was increased to > 90% by reducing space velocity. As shown before, the catalyst deactivated substantially under these conditions showing signs of stabilization at a

relative activity level of ~ 0.4 . At Day 46 under synthesis conditions, the space velocity was increased to the original value used before Day 32. Just as indicated by the model-derived relative activity values obtained at high conversion, a comparison of CO conversions at two-thirds of the original space velocity also showed substantial catalyst deactivation. At Day 48, the catalyst was treated for 8 h at 420 °C in 1.2 MPa flowing H₂. After this treatment, catalytic activity returned close to the fresh lined-out value measured at the beginning of this run segment at Day 32. The nature of the transformation reversing the deactivation caused by hydrothermal conditions at high CO conversion or during water cofeeding will be discussed in the next section in the context of our postrun characterization results.

In another experiment (FBR2_S3), the regenerated catalyst was subjected to > 90% conversion at a higher, 3.5 MPa, total pressure. The catalyst deactivated further (to a relative activity of 0.23) and faster (in 6 days) than at 2.0 MPa (cf. Fig. 4). At higher total pressures, the partial pressure of steam is higher at the same conversion. Therefore, the increased deactivation at increased total pressure is most likely due to this increased steam partial pressure.

We should point out that bulk-phase interparticle condensed water was not present in any of the experiments reported in this study. The calculated steam pressure at 3.5 MPa total pressure and 95% CO conversion with stoichiometric feed, for example, is ≈ 1.0 MPa. This value is less than half of the steam saturation pressure (2.32 MPa) at

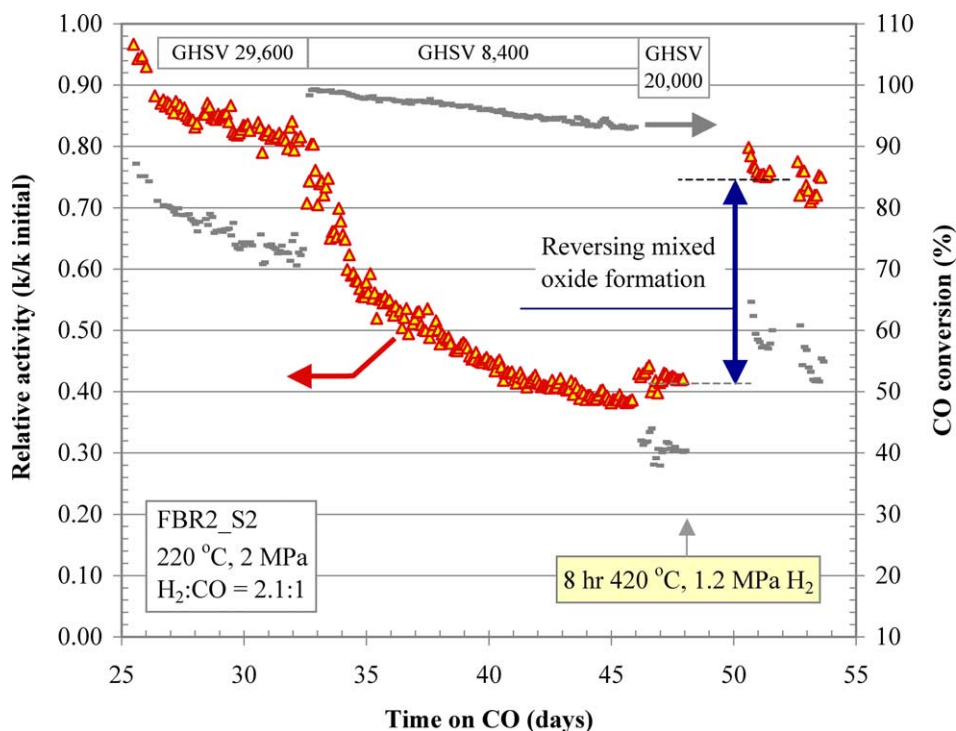


Fig. 4. Deactivation of Co–Re/SiO₂ during high CO conversion with stoichiometric feed (H₂:CO ≈ 2.1:1) and the response of the deactivated catalyst to hydrogen treatment at 420 °C.

the reaction temperature, 220 °C [48]. However, we have no information on the conditions leading to intraparticle pore condensation of water, which therefore cannot be excluded in our experiments.

3.2. Ex situ studies of mixed oxide formation and regeneration

In order to gain a better understanding of the deactivation process observed in the catalytic tests, we performed TEM and EDS characterization of fresh, spent, and steamed fresh samples. First, an aliquot of the crushed fresh 700 °C vacuum-annealed Co–Re/SiO₂ sample was dusted onto a TEM grid and was reduced in flowing H₂ at 425 °C and ambient pressure for 4 h. After reduction, the sample was analyzed by TEM as described under Experimental section. The TEM image of the fresh catalyst (Fig. 5) reveals dense cobalt particle decoration of the silica support owing to the relatively low average cobalt particle size (see particle size distribution in Fig. 6) and high cobalt loading. Note the unimodal particle size distribution, which will bear particular significance in the comparisons with spent catalyst samples.

The spent catalyst sample from the 3.5 MPa catalytic run, FBR2_S3, was hydrogen-treated at the end of the test in the reactor for 1 h at 400 °C and 1.2 MPa to remove the wax from the catalyst bed. The free-flowing mixture of catalyst and quartz diluent was discharged in a N₂-purged glove box. The catalyst was then magnetically separated from the diluent and analyzed by TEM. As opposed to the fresh cata-

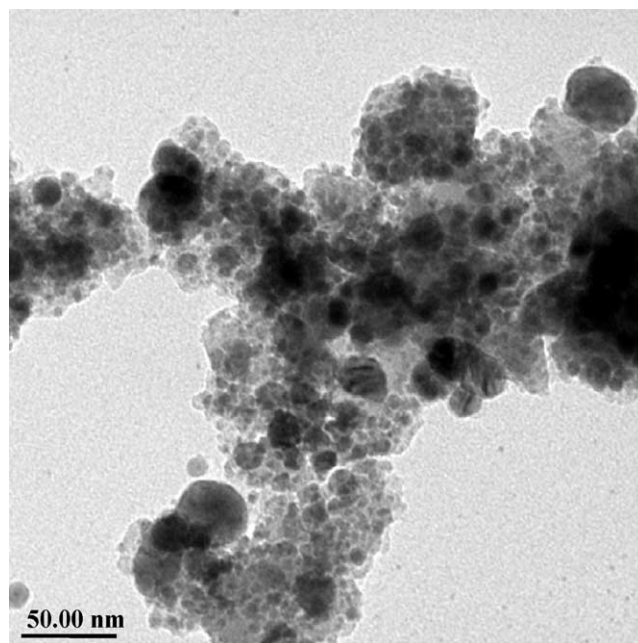


Fig. 5. TEM image of the fresh reduced 700 °C vacuum-annealed Co–Re/SiO₂.

lyst (cf. Fig. 5), the spent catalyst contained a new needle-like phase (see Fig. 7) and cobalt particles with noticeably larger average particle size (compare Figs. 6 and 8). We should mention here that in our experience, the 400 °C hydrogen treatment applied before the catalyst discharge fully re-reduces oxidized cobalt in spent catalysts when the nee-

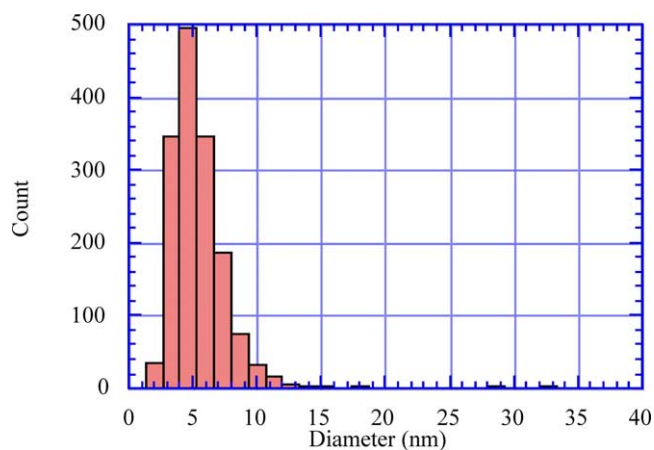


Fig. 6. Cobalt particle size distribution of the fresh reduced 700 °C vacuum-annealed Co-Re/SiO₂.

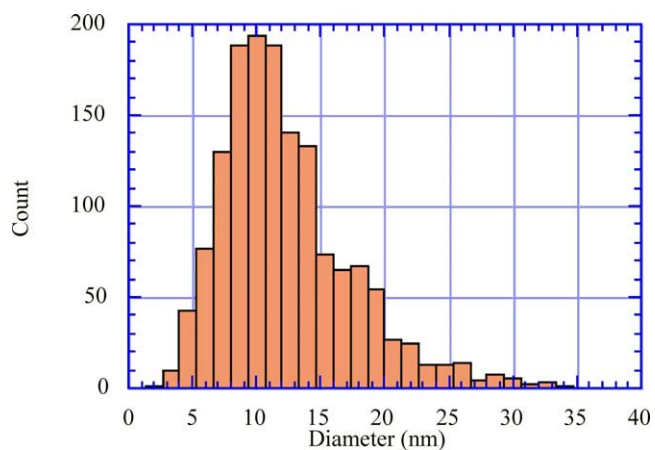


Fig. 8. Cobalt particle size distribution in the spent Co-Re/SiO₂ sample from the 3.5 MPa high CO conversion run.

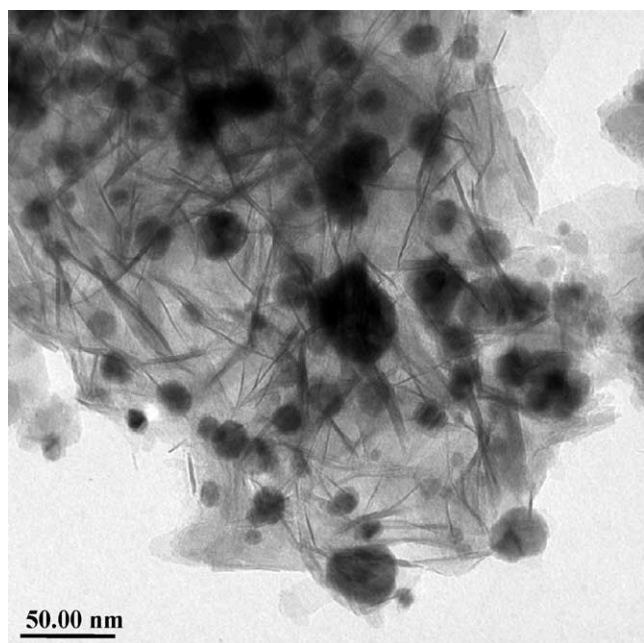


Fig. 7. TEM image of the spent Co-Re/SiO₂ sample from the 3.5 MPa high CO conversion run.

dle phase is not present. However, this hydrogen treatment apparently is not sufficient to decompose the needle phase seen in Fig. 5.

Since the catalytic tests strongly suggested a water-induced transformation of the active cobalt, a reduced sample of the fresh catalyst was steam-treated (for the procedure, see Experimental) to see if a similar transformation could be induced by steam alone. Indeed, we found that the metallic cobalt, clearly visible in the fresh reduced catalyst, mostly disappeared after steaming while copious amounts of a needle phase formed. A comparison of the high-resolution TEM images of the needles in the spent and steamed fresh catalyst samples suggests that the needle-like phases present in these samples are morphologically similar (see Fig. 9): the images depict the same needle morphology with identical (1 nm)

fringe spacing. The fact that the steamed fresh and spent samples have the same needle phase supports our proposal and earlier reports [42–44] that unmodified high surface area silica-supported cobalt catalysts deactivate at the hydrothermal conditions of high-conversion FT synthesis by forming cobalt–silica mixed oxides. It should also be noted that the agent inducing mixed oxide formation is water, and that no other Fischer–Tropsch feed or product component needs to be involved to explain the transformation.

We also attempted the identification of the needle phase in the spent and steamed catalysts by using XRD. As depicted in Fig. 10, there are several unidentified broad peaks in the XRD pattern of the steamed sample that do not belong to cobalt metal, oxide, or hydroxide (e.g., peaks at 2θ of approximately 42, 47, and 60°).⁵ We assign these peaks to the mixed oxide phase observed as needles in the spent and steamed catalysts. Interestingly, none of the cobalt silicate diffraction patterns in our XRD database fit them. Apparently, the needles represent a new cobalt–silica mixed oxide phase.

Since XRD analysis did not provide compositional information, we used energy-dispersive spectrometry to characterize the microscopic needles in the spent FBR2_S3 and in the separately prepared steamed fresh samples. Multiple sampling of several needle crystals in the spent catalyst proved that the new crystalline phase is a well-defined compound: the EDS spectra of all crystal particles are identical (see the three overlapping spectra in Fig. 11). Also, the needle phases in the spent and in the steamed fresh samples were found indistinguishable by EDS yielding the same Co/Si ratio of 1.2:1.0 (see Fig. 12). This finding confirms that the needle phase found in the deactivated catalyst formed in a hydrothermal process induced by steam.

⁵ The diffraction patterns of the spent and steamed samples are similar except for the extra peaks due to the quartz diluent left in the spent sample after magnetic separation. For the sake of clarity, we show and discuss the XRD features of the steamed rather than the spent catalyst.

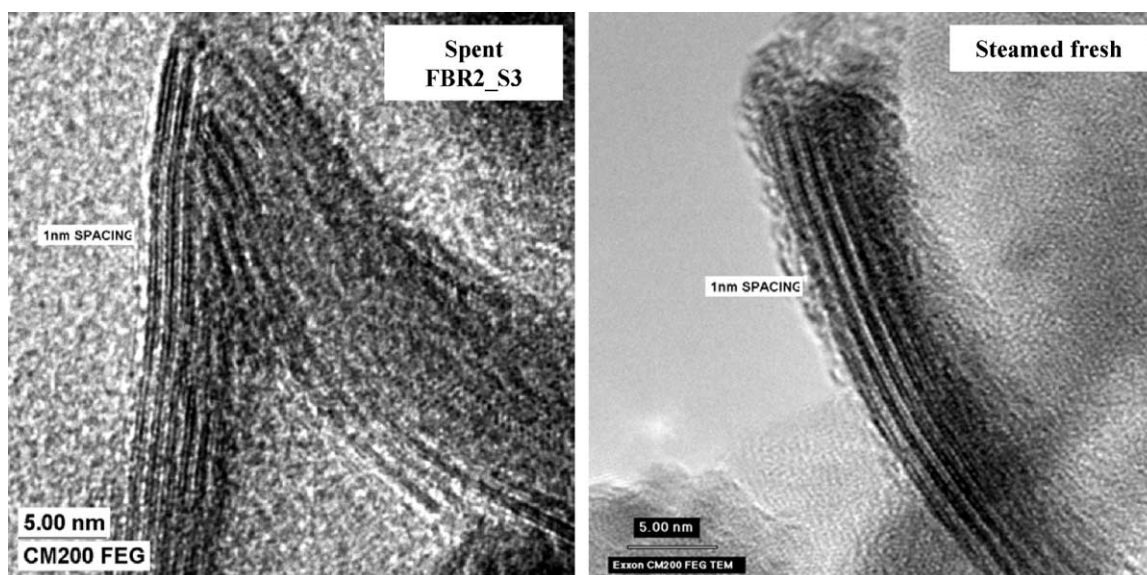


Fig. 9. High-resolution TEM image of the cobalt-silica mixed oxide phase (needles) in the spent Co-Re/SiO₂ sample from the 3.5 MPa high CO conversion run (left) and in the steamed fresh Co-Re/SiO₂ catalyst (right).

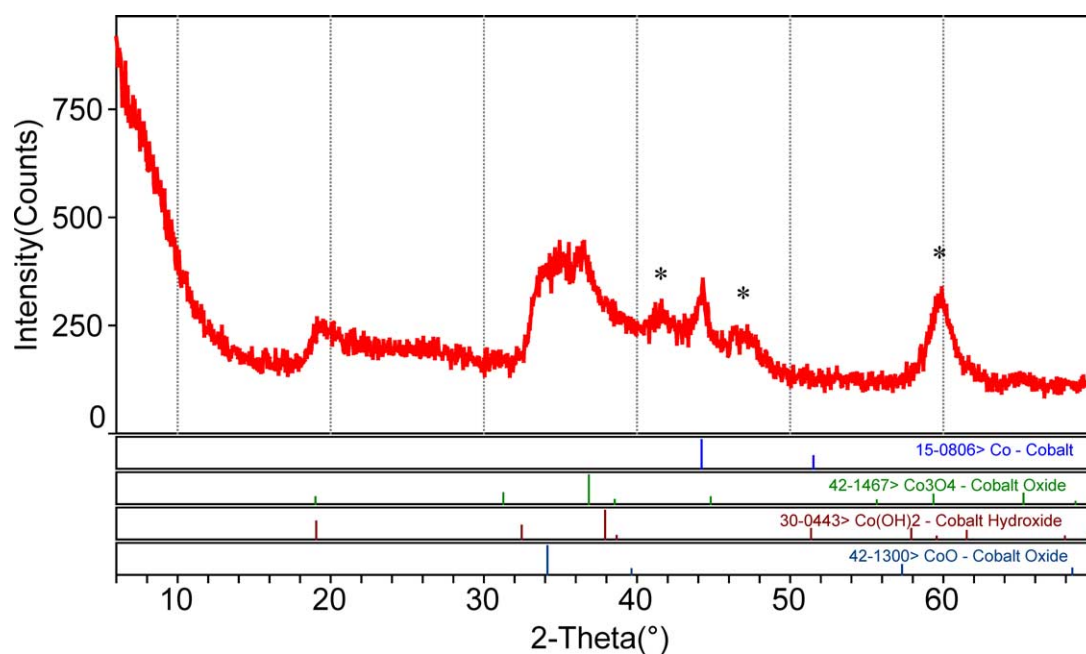


Fig. 10. Powder XRD pattern of the steamed Co-Re/SiO₂ catalyst sample; unidentified peaks that likely belong to the needle phase marked by *.

Although Re and Co are intimately mixed in the fresh catalyst, EDS spectra of the crystalline phase lack any indication of Re. It seems, therefore, that Re does not participate in the formation of the needle phase. Since we did not see any well-defined Re-containing new phase in the spent or steamed samples, it is quite possible that Re does not make a mixed oxide with silica under the conditions that Co does. If it does, the Re-silica mixed oxide is highly dispersed or amorphous, thus invisible in the TEM images. Unfortunately, we do not have analytical data that could resolve the ultimate fate of the Re that was formerly associated with the cobalt forming the mixed oxide. We

suspect that it is present as a highly dispersed oxide at the location of the metal particle from which the mixed oxide crystal formed.

The catalytic tests suggested that high-temperature hydrogen treatment decomposes the cobalt-silica mixed oxide and regenerates the active metallic cobalt. Thus, after examining the mixed oxide containing spent catalyst, the sample on the TEM grid was re-reduced in the microscopy reactor (cf. Experimental) applying high-temperature reduction conditions (12 h, 420 °C, 0.1 MPa H₂). After inertly transferring the sample back into the TEM, an area that was imaged before re-reduction was mapped again to allow a direct

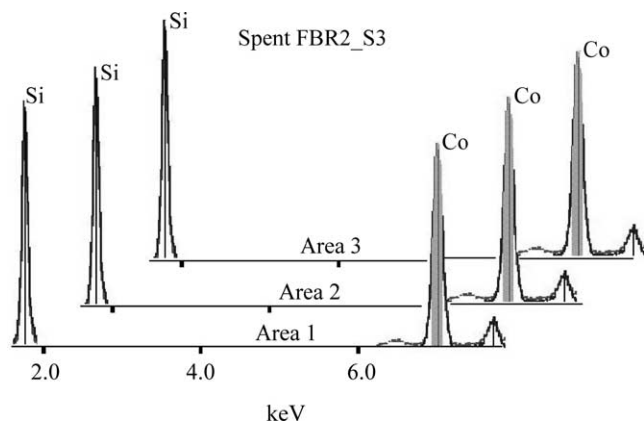


Fig. 11. EDS spectrum of the cobalt-silica mixed oxide phase (needles) in three different needles analyzed in the spent Co-Re/SiO₂ sample from the 3.5 MPa high CO conversion run (FBR2_S3).

comparison of the exact same microscopic features. The images in Fig. 13 demonstrate that the high-temperature hydrogen treatment decomposed most of the needle phase. This ties directly in with our kinetic observations in FBR2_S2 (cf. Fig. 4): high-temperature reductive regeneration restores the active cobalt metal. Noticeably, the re-reduced sample displays not only the large cobalt particles visible in the spent catalyst, but a lot of small metallic cobalt particles as well, while almost all the previously observed needles are missing.

The decomposition of the mixed oxide during high-temperature hydrogen treatment was also examined by TGA. The magnetically separated spent catalyst sample was reduced by heating in atmospheric hydrogen to 500 °C and holding there for 1 h. The TG/DTG curves from the first reduction test (see Fig. 14) indicate the reduction of CoO and Co₃O₄, both below 400 °C. They also reveal a slow third reduction step that starts above 400 °C. Based on the

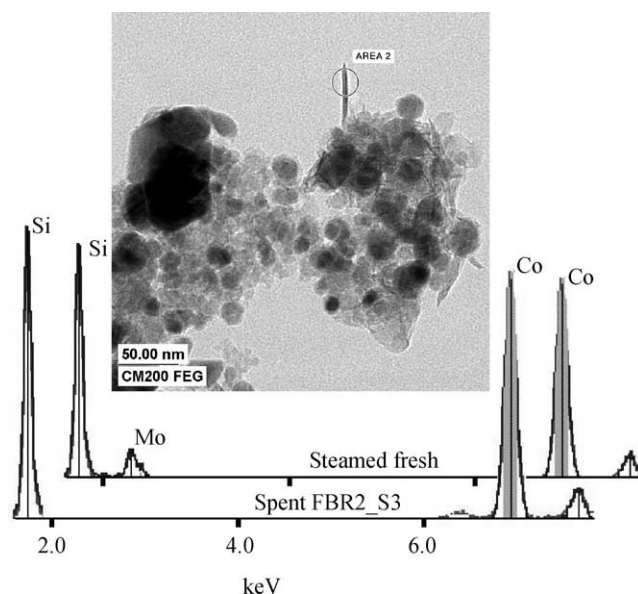


Fig. 12. EDS spectrum of the cobalt-silica mixed oxide phase (needles) in the spent Co-Re/SiO₂ sample from the 3.5 MPa high CO conversion run (FBR2_S3) and in the steamed fresh Co-Re/SiO₂ catalyst. (The Mo signal comes from the TEM grid supporting the steamed fresh sample.)

kinetic and TEM results discussed earlier, we assign this high-temperature weight loss to the decomposition of the mixed oxide needle phase shown in Fig. 7.

It is expected that after the high-temperature regeneration in the first hydrogen treatment, the high-temperature reduction feature would disappear. In order to test this scenario, the reduced sample was first carefully back-oxidized to Co₃O₄, which is the initial state of the fresh calcined sample, and then re-reduced the second time. Indeed, the TG/DTG curves of this second reduction cycle lack the weight loss observed above 400 °C during the first reduction

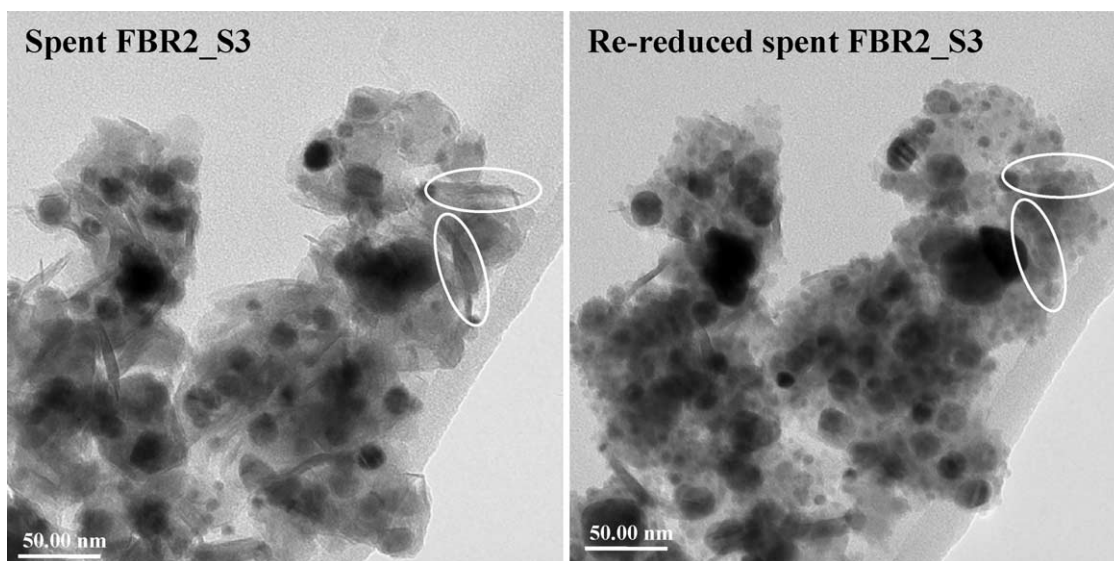


Fig. 13. TEM images of the same area of the spent Co-Re/SiO₂ sample from the 3.5 MPa high CO conversion run (SBR2_S3) before (left) and after (right) hydrogen treatment at 420 °C. Compare areas in white circles showing the disappearance of needles after hydrogen treatment.

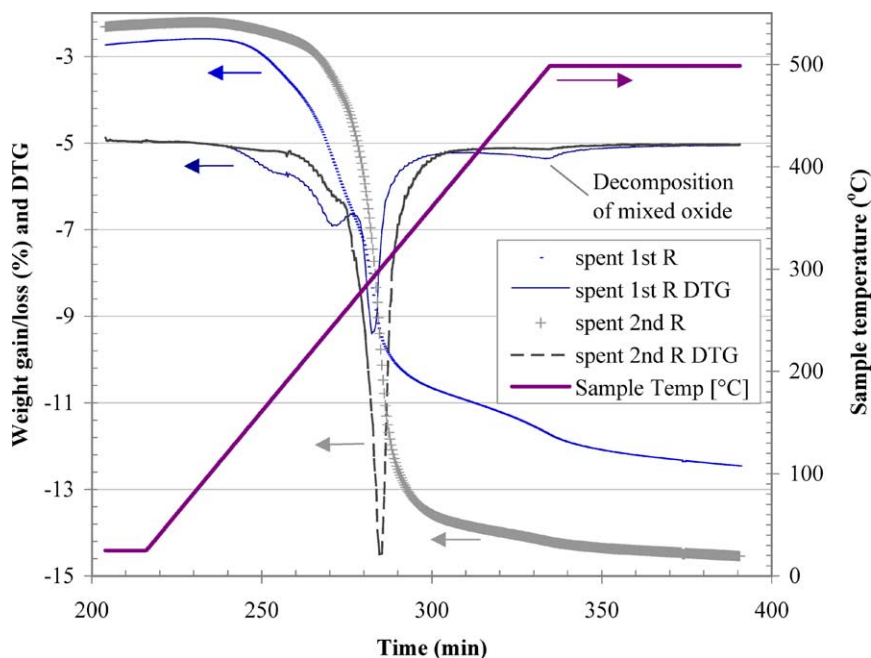


Fig. 14. Thermogravimetric analysis of the spent Co–Re/SiO₂ catalyst containing the cobalt–silica mixed oxide needle phase. Weight losses in the first and second reduction cycle.

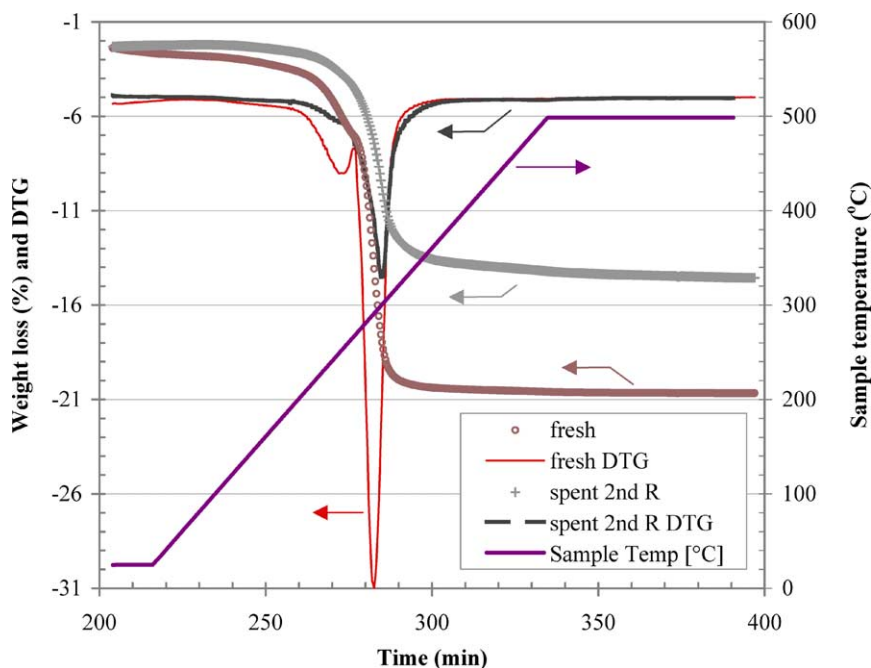


Fig. 15. Thermogravimetric analyses of the fresh and spent Co–Re/SiO₂ catalyst. Weight losses in the third and second reduction cycle, respectively.

(see Fig. 14).⁶ As expected, the high-temperature weight loss is also absent in the TG/DTG trace of the fresh catalyst (see Fig. 15).⁷ Clearly, only the spent catalyst containing the needle phase shows the high-temperature weight loss

providing further indirect evidence for the presence and reducibility of the mixed oxide phase.

The role of Re in the decomposition of the silicate phase during hydrogen treatment is not clear at the moment. Further testing with reduced Re and Re-free catalysts is underway to address this question. We suspect that Re enhances cobalt recovery from the mixed oxide during hydrogen treatment by promoting reduction via hydrogen spillover. In this regard, the studies of Holmen and co-workers [26–28] are very instructive. They reported that

⁶ The difference in the total weight loss during the two reduction cycles is due to the fact that the spent catalyst was not fully back-oxidized.

⁷ The difference in total weight losses observed in Fig. 15 is due to the approximately 34 wt% quartz diluent left in the magnetically separated spent catalyst sample.

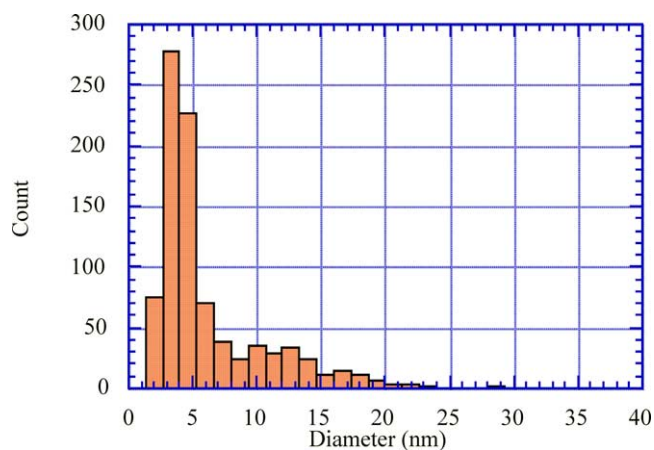


Fig. 16. Cobalt particle size distribution in the spent Co–Re/SiO₂ sample from the 3.5 MPa high CO conversion run after hydrogen treatment at 420 °C.

the cobalt aluminate phase formed during Fischer–Tropsch synthesis in Co–Re/Al₂O₃ catalysts decomposed at lower temperatures than it did in Co only on alumina samples. In this regard, the role of Re is similar to its reduction-promoting effect during the activation of fresh Co–Re catalysts despite of the lack of intimate mixing with cobalt.

Interestingly, the cobalt particle size analysis of the regenerated spent catalyst reveals a bimodal particle size distribution in the re-reduced spent sample (see Fig. 16). Apparently, the total particle population has two subsets: one that was visible as cobalt (metallic or partially oxidized) particles in the spent catalyst sample before high-temperature reduction and another one recovered from the mixed oxide needles (compare Figs. 8 and 16). This later cobalt particle subset has significantly more but smaller particles than the former. High-temperature reduction therefore not only recovers active metal from the inactive mixed oxide but also reduces the average particle size as compared to the spent catalyst. This dual effect can explain the large activity gain after the high-temperature reduction. We should also point out that the mixed oxide formation/re-reduction process can fully explain the deactivation/regeneration process observed in the kinetic tests without invoking deactivation by the often suggested [2–9] carbon buildup and pore-plugging mechanisms.

The bimodal cobalt particle-size distribution could be the result of the interplay of several processes. It is possible, for example, that the mixed oxide needles preferentially form from the small cobalt particles present in the fresh catalyst. If during regeneration the original particle size is not preserved due to, for example, redispersion of the cobalt present in the mixed oxide, bimodal particle size distribution can emerge. Bimodal distribution can also be created if the larger cobalt particles surviving during high conversion agglomerate. The release of smaller particles of the original size (or smaller if redispersion occurred) during reductive regeneration could again introduce bimodal distribution.

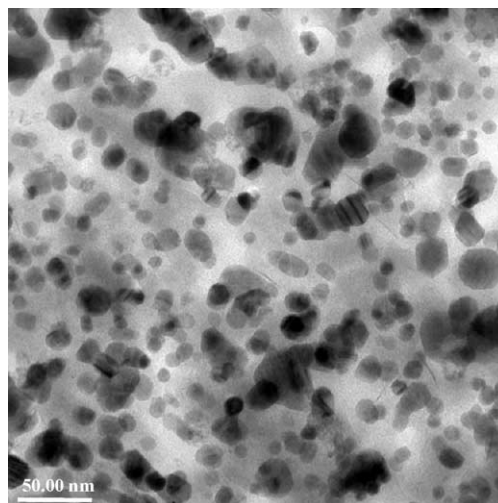


Fig. 17. TEM image of the spent Co–Re/SiO₂ sample from an autoclave Fischer–Tropsch run carried out at moderate (< 80%) CO conversion with stoichiometric feed (H₂:CO ≈ 2.1:1) at 2 MPa and 220 °C.

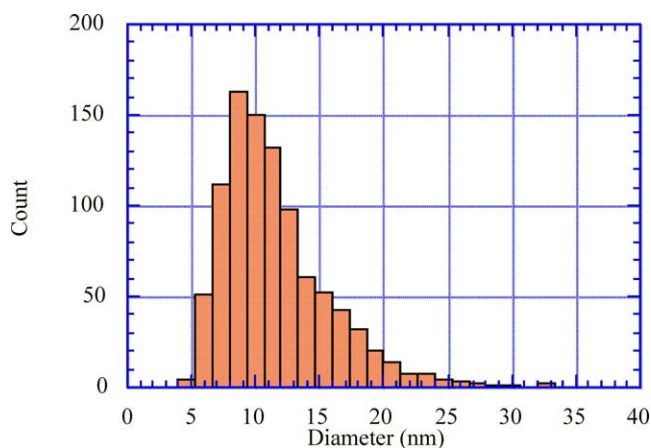


Fig. 18. Cobalt particle size distribution in the spent Co–Re/SiO₂ sample from an autoclave Fischer–Tropsch run carried out at moderate (< 80%) CO conversion with stoichiometric feed (H₂:CO ≈ 2.1:1) at 2 MPa and 220 °C.

Since the bimodal distribution is associated with mixed oxide formation, the particle size distribution of a spent catalyst that was tested under conditions that prevented mixed oxide formation should stay close to unimodal. Figs. 17 and 18 demonstrate that scenario. They show the TEM image and the particle size distribution of a spent Co–Re/SiO₂ sample that was tested in an autoclave at moderate (< 80%) CO conversion levels. The TEM image in Fig. 17 demonstrates the lack of the mixed oxide needle phase. As predicted, the histogram in Fig. 18 reveals a unimodal cobalt particle size distribution in this spent sample.

4. Summary

We found that silica-supported cobalt catalysts deactivate at high water partial pressures created by high CO conversion or steam cofeeding in Fischer–Tropsch synthesis due

to cobalt–silica mixed oxide formation. The tested fumed silica-supported cobalt catalyst formed a needle-like crystalline cobalt–silica mixed oxide causing rapid deactivation at high (> 90%) CO conversion with stoichiometric feeds at 220 °C and ≥ 2 MPa total pressures.

The morphology and composition of the deactivation-causing mixed oxide in the spent catalyst were the same as those found in steamed fresh samples suggesting a hydrothermal deactivation process induced at high steam pressure. Although low-temperature (225 °C) hydrogen treatment did not recover cobalt from this mixed oxide phase, cobalt was regenerated, and thus catalytic activity restored, by high-temperature (≥ 400 °C) reduction in flowing H₂ at 1.2 MPa.

The cobalt particle size distribution was bimodal in the reductively regenerated catalyst showing an increased population of small particles. This observation suggests that the cobalt–silica mixed oxide phase preferentially formed from the small cobalt particles present in the fresh catalyst.

Acknowledgments

The authors thank Prof. Enrique Iglesia (UC Berkeley), Dr. LeRoy Clavenna, Dr. Mark M. Disko, Dr. John L. Robbins, and Dr. Stuart L. Soled (all from ExxonMobil Res. & Eng. Co.) for the insightful discussions. We also acknowledge Mrs. Maria Oliva-Duran for the technical assistance, and Mr. Sabato Miseo and Dr. Soled for the XRD analysis (all from ExxonMobil Res. & Eng. Co.).

References

- [1] P.J. van Berge, R.C. Everson, *Stud. Surf. Sci. Catal.* 107 (1997) 207–212.
- [2] H.W. Pennline, S.S. Pollack, *Ind. Eng. Chem. Prod. Res. Dev.* 25 (1986) 11–14.
- [3] D.-K. Lee, J.-H. Lee, S.-K. Ihm, *Appl. Catal.* 36 (1988) 199–207.
- [4] H.W. Pennline, R.J. Gormley, R.R. Schehl, *Ind. Eng. Chem. Prod. Res. Dev.* 23 (1984) 388–393.
- [5] P.K. Agrawal, J.R. Katzer, W.H. Manogue, *J. Catal.* 69 (1981) 312–326.
- [6] M.K. Niemela, A.O.I. Krause, *Catal. Lett.* 42 (1996) 161–166.
- [7] S.L. Soled, E. Iglesia, R. Fiato, G.B. Ansell, US patent 5,397,806, 1995.
- [8] E. Iglesia, S.L. Soled, R.A. Fiato, G.H. Via, *J. Catal.* 143 (1993) 345–368.
- [9] C.H. Mauldin, S.M. Davis, K.B. Arcuri, US patent 4,755,536, 1988.
- [10] U. Kestel, G. Frohlich, D. Borgmann, G. Wedler, *Chem. Eng. Technol.* 17 (1994) 390–396.
- [11] C.J. Bertole, C.A. Mims, G. Kiss, *J. Catal.* 210 (2002) 84–96.
- [12] A.M. Hilmen, O.A. Lindvag, E. Bergene, D. Schanke, S. Eri, A. Holmen, *Stud. Surf. Sci. Catal.* 136 (2001) 295–300.
- [13] E. Iglesia, *Appl. Catal. A: Gen.* 161 (1997) 59–78.
- [14] H. Schulz, M. Claeys, S. Harms, *Stud. Surf. Sci. Catal.* 107 (1997) 193–200.
- [15] E. Iglesia, in: E. Herrero, O. Anunziata, C. Perez (Eds.), *Proceedings XV Iberoamerican Catal. Symp., Plenary Address*, 1996, pp. 17–36.
- [16] H. Schulz, E. van Steen, M. Claeys, *Stud. Surf. Sci. Catal.* 81 (1994) 455–460.
- [17] H.P. Withers, K.F. Eliezer, J.W. Mitchell, *Ind. Eng. Chem. Res.* 29 (1990) 1807–1814.
- [18] C.J. Kim, US patent 5,227,407, 1993.
- [19] C.J. Kim, Eur. patent 0,355,218, 1990.
- [20] C.J. Kim, Eur. patent 0,339,923, 1989.
- [21] E. Iglesia, R. Madon, US patent 4,754,092, 1988.
- [22] J.K. Minderhoud, M.F.M. Post, S.T. Sie, S.T.S. Sudholter, US patent 4,628,133, 1986.
- [23] P.J. van Berge, J. van de Loosdrecht, S. Barradas, A.M. van der Kraan, *Catal. Today* 58 (2000) 321–334.
- [24] P.J. van Berge, J. van de Loosdrecht, S. Barradas, A.M. van der Kraan, *Prepr.—Am. Chem. Soc., Div. Pet. Chem.* 44 (1999) 84–87.
- [25] F. Rohr, A. Holmen, E.A. Blekkan, *Prepr.—Am. Chem. Soc., Div. Pet. Chem.* 44 (1999) 73–75.
- [26] A.M. Hilmen, D. Schanke, K.F. Hanssen, A. Holmen, *Appl. Catal. A: Gen.* 186 (1999) 169–188.
- [27] M. Rothaemel, K.F. Hanssen, E.A. Blekkan, D. Schanke, A. Holmen, *Catal. Today* 38 (1997) 79–84.
- [28] K.F. Hanssen, E.A. Blekkan, D. Schanke, A. Holmen, *Stud. Surf. Sci. Catal.* 109 (1997) 193–202.
- [29] D. Schanke, A.M. Hilmen, E. Bergene, K. Kinnari, E. Rytter, E. Adnanes, A. Holmen, *Energy Fuels* 10 (1996) 867–872.
- [30] D. Schanke, A.M. Hilmen, E. Bergene, K. Kinnari, E. Rytter, E. Adnanes, A. Holmen, in: *ACS Div. of Fuel Chem. Preprints, 209th ACS Natl. Mtg., Anaheim, CA, Vol. 40, 1995*, pp. 167–171.
- [31] D. Schanke, A.M. Hilmen, E. Bergene, K. Kinnari, E. Rytter, E. Adnanes, A. Holmen, *Catal. Lett.* 34 (1995) 269–284.
- [32] G. Jacobs, Y. Zhang, T.K. Das, J. Li, P.M. Patterson, B.H. Davis, in: *Proceedings, 9th Int. Symp. on Cat. Deact.* Lexington, KY (October 7–10, 2001), 2001, pp. 415–422.
- [33] F. Rohr, O.A. Lindvag, A. Holmen, E.A. Blekkan, *Catal. Today* 58 (2000) 247–254.
- [34] J.M. Jablonski, M. Wolczyk, L. Krajczyk, *J. Catal.* 173 (1998) 530–534.
- [35] E. van Steen, G.S. Sewel, R.A. Makhothe, C. Micklethwaite, H. Manstein, M. de Lange, C.T. O'Connor, *J. Catal.* 162 (1996) 220–229.
- [36] G.J. Haddad, J.G. Goodwin Jr., *J. Catal.* 157 (1995) 25–34.
- [37] H. Ming, B.G. Baker, *Appl. Catal. A: Gen.* 123 (1995) 23–36.
- [38] K.E. Coulter, A.G. Sault, *J. Catal.* 154 (1995) 56–64.
- [39] I. Puskas, T.H. Fleisch, J.B. Hall, B.L. Meyers, R.T. Roginski, *J. Catal.* 134 (1992) 615–628.
- [40] B. Viswanathan, R. Gopalakrishnan, *J. Catal.* 99 (1986) 342–348.
- [41] A. Hoek, J.K. Minderhout, P.W. Lednor, Eur. patent 110,449, 1983.
- [42] A. Barbier, A. Tuel, I. Arcon, Kodre, G.A. Martin, *J. Catal.* 200 (2001) 106–116.
- [43] G.W. Huber, C.G. Guymon, T.L. Conrad, B.C. Stephenson, C.H. Bartholomew, in: *Proceedings, 9th Int. Symp. on Cat. Deact.* Lexington, KY (October 7–10, 2001), 2001, pp. 423–430.
- [44] A. Kogelbauer, J.C. Weber, J.G. Goodwin Jr., *Catal. Lett.* 34 (1995) 259–267.
- [45] C.K. Kliewer, M.M. Disko, S.L. Soled, G.J. DeMartin, *Proc. Microsc. Microanal. (Suppl. 2)* 5 (1999) 926.
- [46] D. Schanke, K.J. Kinnari, GB 2,299,767, 1996.
- [47] A. Hoek, J.H. Moors, WO 97/17137, 1997.
- [48] R.C. Weast (Ed.), *CRC Handbook of Chemistry and Physics*, 67th ed., CRC Press, Boca Raton, FL, 1986–1987, pp. 16–23.
- [49] C.H. Mauldin, D.E. Varnado, *Stud. Surf. Sci. Catal.* 136 (2001) 417.
- [50] C.J. Bertole, C.A. Mims, G. Kiss, *J. Catal.* 210 (2002) 84.
- [51] C.J. Bertole, C.A. Mims, G. Kiss, P. Joshi, *Stud. Surf. Sci. Catal.* 136 (2001) 369.